# Precipitation behavior during high-temperature isothermal compressive deformation of Inconel 718 alloy

**Hongjun Zhang, Chong Li, Yongchang Liu*, QianyingGuo, Huijun Li**

State Key Lab of Hydraulic Engineering Simulation and Safety, School of Materials Science & Engineering, Tianjin University, Tianjin 300072, PR China

**Abstract:** The precipitation behaviors of γ″ and δ phases during high-temperature isothermal compressive deformation of Inconel 718 alloy are investigated under the strain rate of $2.2 \cdot 10^{-4}$ $s^{-1}$. It is found that the precipitation behaviors are tailored by deformation temperatures, and lead to the disparately abnormal deformation characteristics. Under the deformation temperature of 800°C, the microstructure is composed of incoherent needle-shaped γ″ precipitates at grain boundaries and ultrafine spherical γ″ particles within grains, resulting in the exceptional decrease of flow stress with absence of DRX. When deformed at 900 °C, it becomes needle-shaped δ precipitates at grain boundaries and intragranular disc-shaped γ″ precipitates, and the DRX softening degree is lowered consequently.

**Keywords:** γ″-phase, δ-phase, Precipitation behaviors, Isothermal deformation, Inconel 718 alloy

## 1. Introduction

Due to its excellent mechanical properties as well as good corrosion resistance at high temperature up to 650 °C, the nickel-based Inconel 718 alloy has been widely used for manufacturing high temperature components (turbine, compressor disk, blade and vane, etc.) in the aerospace industry [1,2]. Generally, Inconel 718 alloy is strengthened by the precipitation of metastable γ′ ($Ni_3Al$) coupled with γ″ ($Ni_3Nb$) phases and the coherent disc-shaped γ″-phase is the major strengthening phase [3,4]. The orthorhombic incoherent δ-phase ($Ni_3Nb$) is the equilibrium phase corresponding to γ″-phase, which has higher stability at elevated temperature [5].

In the manufacturing processes of the high temperature components used in aircraft, Inconel 718 alloy often needs to be hot deformed to meet the strict requirements of microstructure and mechanical properties. The microstructure and mechanical properties is sensitive to the deformation parameters, and the microstructural evolution during the deformation in turn affects the flow behaviors [6]. Thus, it is valuable to understand the flow behaviors and microstructural evolution in the hot deformation of Inconel 718 alloy. In recent years, many efforts have been made to investigate the hot deformation behaviors of Inconel 718 alloy [7-16], and the previous studies are mainly focused on the flow behaviors, dynamic recrystallization (DRX), processing maps. However, little attention were paid on the second-phase precipitation during high-temperature deformation. Generally, the high-temperature properties of Inconel 718 alloy are determined by the quantity and morphology of γ′, γ″ and δ precipitates. For the wrought Inconel 718 alloy, the thermo-processing parameters (deformation temperature, strain rate, deformation degree, etc.) have great influences on the precipitation of γ′, γ″ and δ phases. The second-phases precipitated during deformation not only affect the flow behaviors and workability, but also

influence the precipitation behaviors in the following aging process and mechanical properties [17]. Therefore, it is of significance to investigate the second-phase precipitation behaviors during hot deformation of Inconel 718 alloy.

In this study, the precipitation behaviors of γ″ and δ phases during isothermal compressive deformation of Inconel 718 alloy are investigated. The compressive tests are conducted under the strain rate of $2.2 \cdot 10^{-4}$ $s^{-1}$ during the deformation time of 1h, at the two different deformation temperatures of 800 °C and 900 °C, which are characterized in the range of γ″ and δ-phase precipitation temperatures respectively. The disparately abnormal deformation characteristics are illustrated, and the varied precipitation behaviors of γ″ and δ phases are analyzed. Based on the experimental results, the effects of transformation of γ″ and δ phases during deformation on the flow behaviors are discussed.

## 2. Experimental

The experimental materials used in this study is a commercial Inconel 718 alloy provided by BaoSteel, and its chemical composition (wt.%) is: 52.63Ni-19.00Cr-5.05(Nb+Ta)-3.09 Mo-1.02Ti -0.51Al-0.02Co-0.02C-(bal.)Fe. Cylindrical specimens with a diameter of 8 mm and a height of 12 mm were cut from the wrought bar. The specimens were first solution treated at 1050 °C for 60 min and then cooled to room temperature in air, which were defined as ST specimen. The original microstructure of the material after solution treatment is composed of equiaxed grains with mean size of 136 μm as well as some twins, as shown in Fig. 1. Hot compressive tests were conducted under the strain rate of $2.2 \cdot 10^{-4}$ $s^{-1}$ in 1h at the temperatures of 800 °C and 900 °C, which were defined as 800-HD and 900-HD specimen respectively, and the technical parameters are shown in Fig. 2. As a result, the height reduction of cylindrical specimens is about 50%,

The hot compressive tests were performed on a Gleeble-3500 thermo mechanical simulator. Before compressive deformation, specimens were heated to the designed temperature at a rate of 10 °C/s and then soaked for 2 min to reduce the thermal gradient. After the deformation, specimens were subsequently quenched by water at a cooling rate fast enough to avoid precipitation, and the error range of temperature were ±2 °C. In order to reduce the friction and avoid the adhesion, tantalum foils with the thickness of 0.1 mm were placed between the specimen and dies. In addition, specimens were cut along the compression axis section, mechanically polished, then chemical etched for 8~10 min with a solution consist of 5g $CuCl_2$ + 100 ml HCl + 100 ml $CH_3CH_2OH$ at room temperature. The microstructure and morphologies of precipitates were examined using optical microscope (OM), scanning electron microscope (SEM) with the voltage of 20kV, and X-ray diffraction spectra (XRD) of different specimens were measured by D8 Advanced diffractometer. Differential scanning calorimetry (DSC) experiments were performed at the heating rate of 30 °C/min to limit the precipitation during the heating procedure as much as possible. The grain sizes were measured by the Image Pro-Plus software 6.0. Transmission electron microscope (TEM) observations were performed to analyze the dislocation substructures in the deformed specimens. Specimens for TEM observations were firstly machined from the deformed specimens, then grinded into 70~80 μm thick foils, and electro-polished using a solution of 10% $HClO_4$ and 90% $CH_3CH_2OH$.

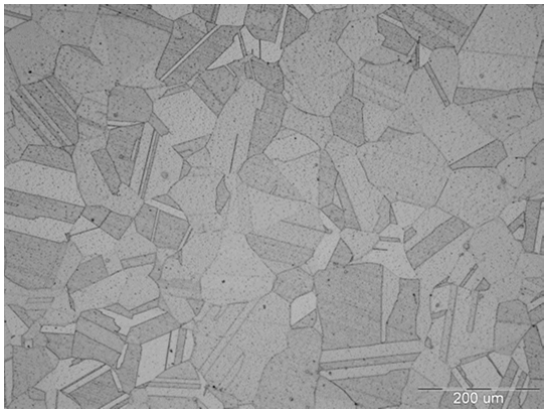


**Fig. 1. Optical morphology of solution-treated Inconel 718 alloy before hot deformation**

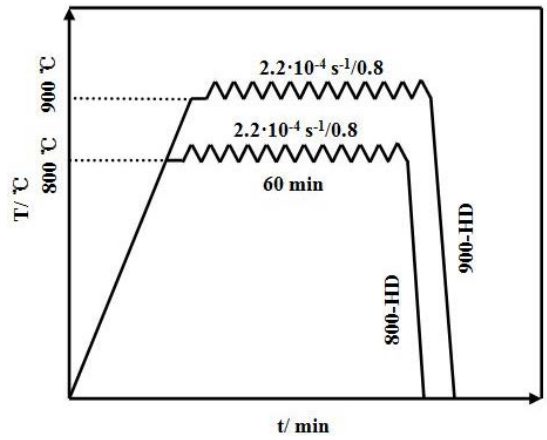


**Fig. 2. Schematic diagrams of different deformation processes**

## 3. Results and discussions

### 3.1 Hot compressive deformation characteristics

As shown in Fig. 3, the true stress-strain curves have revealed two significantly disparate deformation characteristics. At the initial stage of deformation, the main deformation mechanisms are work hardening and dynamic recovery. However, the dynamic recovery is so weak due to the relatively low stacking fault energy of Inconel 718 alloy as well as the low strain rate that cannot overcome the work hardening [18]. Hence, the flow stress increases rapidly at the initial stage of both specimens. Afterwards, it exhibits two different flow behaviors after peak stress with further straining, that obvious decrease and unnoticeable softening for 800-HD and 900-HD, respectively.

The DRX temperature of Inconel 718 alloy is about 850 $^{o}$C [19]. Seen from the OM morphology of 800-HD specimen shown in Fig. 4(a), no DRX grains are observed. According to the DSC curve in Fig. 5, the peak temperature of γ″-phase precipitation for the explored Inconel 718 alloy is about 804 $^{o}$C, which is similar to the results of Ref. [21,22]. Thus, it can be inferred

that γ″-phase will precipitate during the deformation procedure of 1h at 800 °C. In this case, the flow stress of 800-HD specimen is mainly determined by the comprehensive effects of work hardening, second-phase precipitation and dynamic recovery. In the absence of DRX, the abnormal rapidly decrease of flow stress after peak stress may be attributed to the second-phase precipitation.

A number of fine DRX grains are observed at the deformed grain boundaries of 900-HD specimen, as depicted in Fig. 4(b). According to the DSC curve in Fig. 5, 900 °C is higher than the onset temperature of the δ-phase precipitation. Hence, the flow stress of 900-HD specimen is mainly determined by the comprehensive effects of work hardening, DRX, second-phase precipitation and dynamic recovery. Whereas, the flow stress exhibits a relatively unnoticeable softening after peak stress in the presence of DRX. Therefore, the second-phase precipitation is supposed to be responsible for the abnormal stability of flow stress.

As illustrated above, the exceptional flow behaviors are discovered in the isothermal compressive deformations at two temperatures, and the causes are identified as the second-phase precipitation. Therefore, the precipitation behaviors during the deformations are to be investigated in the following sections.

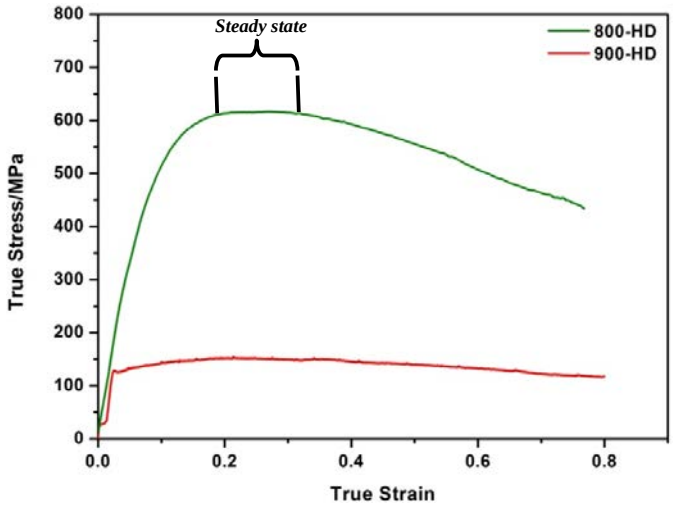


**Fig. 3. True stress-strain curves for the explored Inconel 718 alloy**

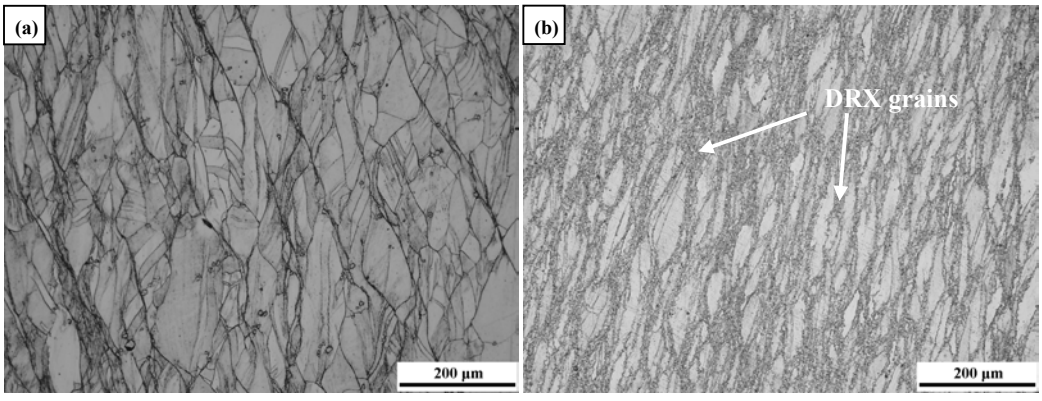


**Fig. 4. OM morphologies of (a) 800-HD, and (b) 900-HD**

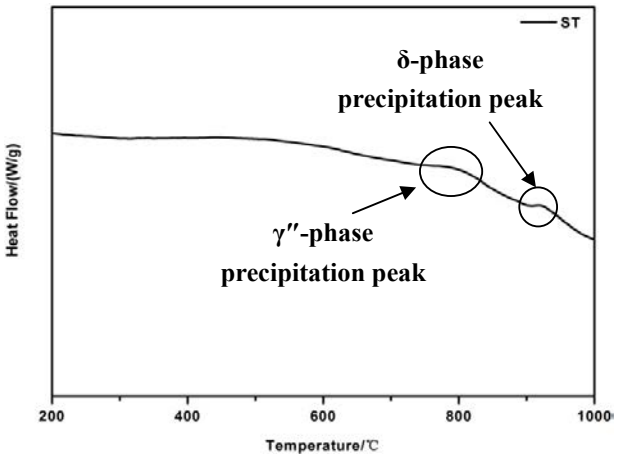


**Fig. 5. DSC curve of solution treated specimen**

### 3.2 Precipitation behaviors during isothermal compressive deformation

As depicted in Fig. 6(a), the original grains are elongated along the vertical axis section for 800-HD specimen, and some large-sized blocky NbC-carbides are located at the vicinities of broadened grain boundaries. Under higher magnification (see Fig. 6(b)), it is observed that some needle-shaped γ″ precipitates are located at grain boundary, of which average size in length is ~400 nm and 20~40 nm in thickness. Simultaneously, plenty of ultrafine spherical γ″ particles with mean radius of few tens of nanometers are distributed homogeneously in grain interior (see Fig. 6(c)).

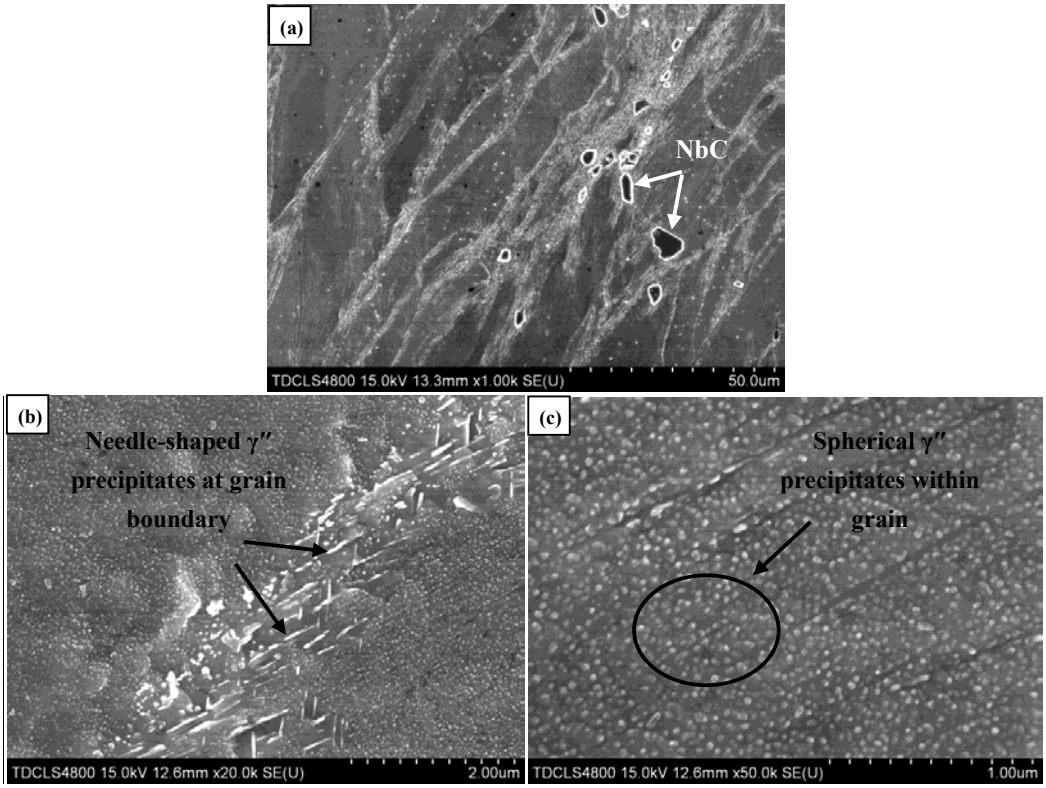

**Fig. 6. SEM morphologies of 800-HD specimen under different magnifications. (a) showing the elongated original grains and NbC-carbides,** ×1.00 k **(b) indicating the needle-shaped γ″ precipitates at grain boundary,** ×20.0 k **(c) demonstrating the ultrafine spherical γ″ particles within grains,** ×50.0 k.

During continuously compressive deformation, dislocations are motivated to slip and climb, leading to the generation and propagation [20]. The motioned dislocations will be hindered by grain boundary (GB), then piled up [1,23]. On the one hand, the GB-dislocations can provide favorable positions for the nucleation of γ″-phase. On the other hand, the strain energy stored in dislocations i.e. the dislocation storage energy may reduce the critical nucleation energy of γ″-phase. In this way, γ″-phase will nucleate preferentially on the piled-up dislocations at grain boundaries during deformation, and the nucleation process is finished in few minutes [24]. In addition, the dislocation storage energy can provide driving force for γ″-phase growth, and the dislocation network can supply adequate accesses for Nb-atoms diffusion to improve its diffusion efficiency. As the growth of γ″-phase is mainly controlled by the volume diffusion of Nb-atoms in matrix [25,26], so the growth of γ″ nuclei is enhanced to a large extend.

The transition of γ″-phase morphology during growth is mainly determined by minimizing the global energy of the system [27]. On account of the weak dynamic recovery of Inconel 718 alloy, the GB-dislocation storage energy may get released mainly through providing driving energy for γ″-phase growth. Consequently, the global energy of the system is improved. The global energy can be reduced to the chemical free energy, interfacial energy due to the interface between γ and γ″ precipitates and elastic distortion energy associated with the lattice misfit [28]. With γ″ nuclei growing in size, the lattice misfit between γ-matrix is increased, and its coherence is decreased. Responding to the increased lattice misfit, the elastic distortion energy is increased. Under the principle of minimizing the global energy of the system, the γ″-phase morphology will be changed to reduce the interfacial energy for offsetting the increase of global energy during the growth process. As a result, the morphology of γ″-phase becomes unstable. In order to accommodate lower interfacial energy, the morphology of γ″-phase is transformed from the initial sphere to disc-shape, and the disc-shape tends to adopt smaller values for its aspect ratio $q= e/L$ when their length increases with time, where $L$ is the diameter of the disc-shaped particle, $q = e/L$ is the aspect ratio, where $e$ is the thickness of the disc [29]. As reported by Slama et al. [30], γ″-phases were incoherent when the diameter $L$ reached a value of 120 nm in Inconel 718 alloy. For 800-HD specimen in this work, the mean $L$ value of GB-γ″ precipitates is ＞400 nm, which have lost coherence with matrix, leading to the high elastic distortion energy. Under this condition, the morphology of disc-shaped γ″-phase gets evolved by means of increase in $L$ and decrease in $e$ largely, resulting in the needle-shape to lower interfacial energy sufficiently.

During the deformation at 800 $^{o}$C in 1h, γ″-phase can nucleate uniformly within grains since 800 $^{o}$C is near the γ″-phase precipitation peak temperature for the studied Inconel 718 alloy. However, there are much less dislocations in grain interior due to the low strain rate of $2.2\cdot10^{-4}$ $s^{-1}$ as well as dynamic recovery. The diffusion rate of Nb-atoms in the γ-matrix and the driving force for growth of intragranular γ″ precipitates are reduced greatly attributed to the much lower dislocation density within grains. In this way, the interfacial energy becomes dominant. As reported by Devaus et al. [29], the interfacial energy of γ″/γ (95±17mJ $m^{-2}$) is far too lower than the activation energy of γ″ coarsening (272 kJ $mol^{-1}$) in Inconel 718 alloy, so the growth of

intragranular γ″ nuclei is inhibited and its morphology becomes stable. As a consequence, numerous ultrafine γ″ particles precipitate homogeneously with initial spherical morphology in the grain interior.

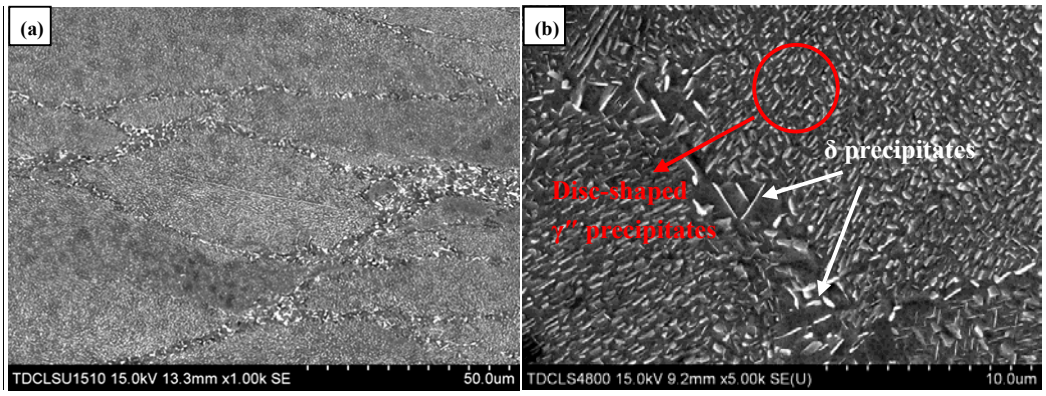


**Fig. 7. SEM morphologies of 900-HD specimen under different magnifications**

But, the microstructure of 900-HD specimen displays a kind of remarkably different morphology, which is composed of some large-sized δ precipitates located at grain boundaries and uniformly distributed coarse γ″ precipitates within grains, seen distinctly in Fig. 7(a) under a relatively low magnification. The sparse GB-δ precipitates exist in shapes of needle or short-rod, and the orientations are diverse and irregular, as shown in Fig. 7(b). At the initial stage of deformation, the number of GB-dislocations is increased, and DRX occurs when it reaches the critical dislocation density [31]. Part of the piled-up dislocations at initial grain boundary are annihilated under the effect of DRX, and the retained dislocations are rearranged to pile up at the boundary of fresh DRX grains [23], as presented in Fig. 8(a). The δ-phase precipitation onset temperature of the explored Inconel 718 alloy is calculated to be about 898 $^{o}$C from the DSC results in Fig.5. According to the PTT diagram of Inconel 718 alloy presented by Thomas et al. [32], δ-phase may precipitate only at grain boundary in 1 h at 900 $^{o}$C. Otherwise, δ-phase is mainly transformed from γ″-phase when aging at 900 $^{o}$C, and the piled-up dislocations at DRX grain boundary will accelerate the γ″→δ transformation [22]. Consequently, δ-phase precipitated at the DRX grain boundary, and developed along the elongated orientation to restrain the growth of DRX grain, separating the original grain boundary into lots of sub-units.

It is observed that there are plenty of anomalously coarse γ″ precipitates distributing uniformly within the deformed original grains of 900-HD specimen, as shown in Fig. 7(b) under a higher magnification. The appearance of intragranular γ″-phase is defined as disc-shape, and the mean diameter $L$ is calculated to be larger than 500 nm. Thus, it is believed that the deformation temperature has great influences on the γ″-phase precipitation. The dislocations are accumulated continuously in the matrix during deformation, and the propagated dislocations get tangled with each other, resulting in the formation of irregular dislocation network, as illustrated in the TEM morphology of Fig. 8(b). As stated above, the dislocations can not only provide favorable sites for γ″-phase nucleation but also reduce its critical nucleation energy, stimulating its precipitation in the matrix. The tangled dislocations can serve as the pipes for the diffusion of γ″-forming elements, enhancing the diffusion efficiency of Nb-atoms. As the coarsening behavior of γ″-phase in Inconel 718 alloy is mainly controlled by the volume diffusion of niobium in the matrix [32,33], the

intragranular γ″-phase nuclei can grow rapidly owing to the promoted niobium diffusion at 900 °C. In addition, due to the relatively lower dislocation density compared with the grain boundary, as well as the high coherence between γ″-phase and γ-matrix, the γ″→δ transformation is suppressed in the interior of deformed original grains. Consequently, the γ″ nuclei grow rapidly into the stable disc-shape. Moreover, it can be surmised that the dislocation density has vital effects on the γ″→δ transformation, which need to be investigated further.

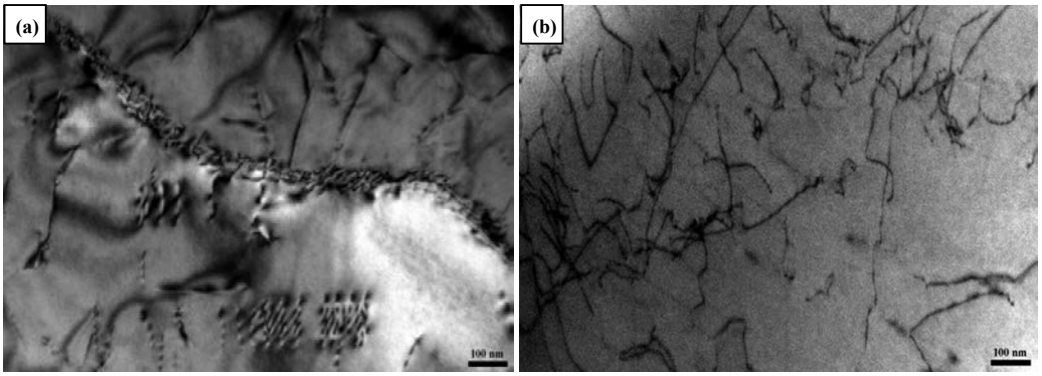


**Fig. 8. The dislocation distribution morphologies of 900-HD specimen. (a) indicating that massive dislocations piled up at the original grain boundary, separating into lots of sub-units which refers to DRX grains, (b) showing the tangled dislocations within deformed original grains.**

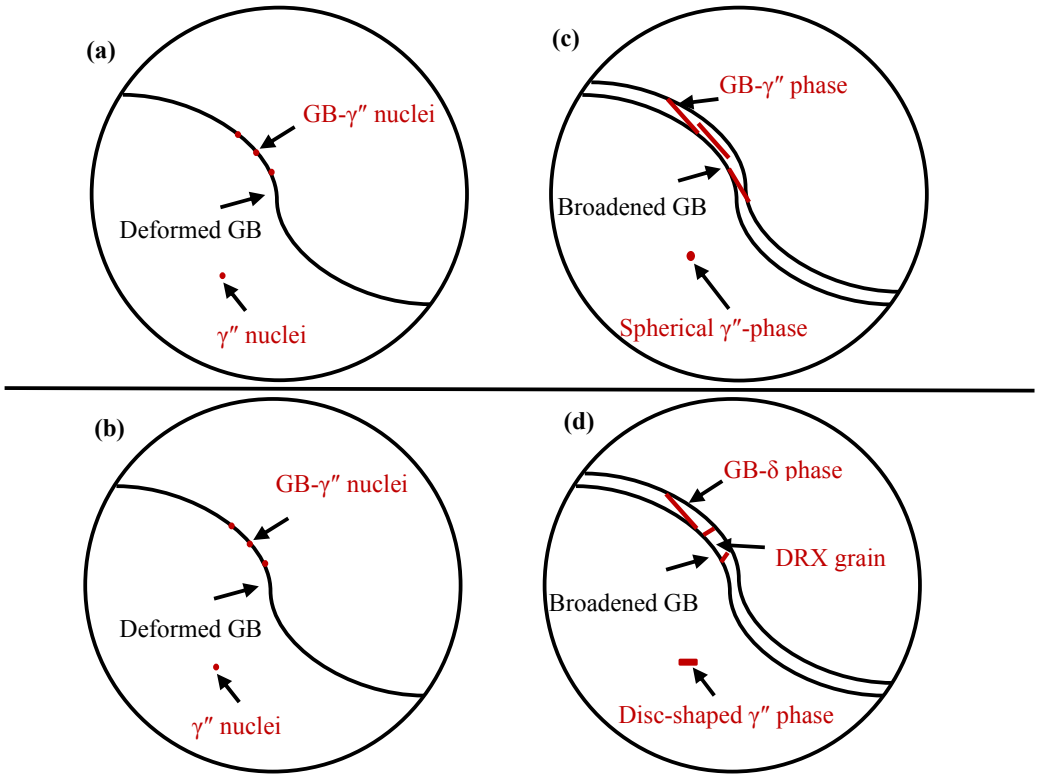

**Fig. 9. Schematic diagrams for precipitation behavior during deformation at 800 $^{o}$C (a, c) and 900 $^{o}$C (b, d). (a), (b) at the initial stage of deformation; (c), (d) at the true strain of 0.8.**

Schematic diagrams are made to illustrate the varied precipitation behaviors stated above, as shown in Fig. 9. At the initial stage of deformation, γ″-phase nucleates at deformed grain boundaries and within grains in few minutes. With further straining, the grain boundary is broadened, and the coherently generated spherical γ″ nuclei will exhibit growth along with proper morphology transition. After deformation in 1h at 800 $^{o}$C, the GB-γ″ nuclei grow into incoherently needle-shaped γ″ phases. Whereas, the intragranular γ″ nuclei appear little changes, and ultrafine spherical γ″ particles are observed in grain interior. When deformed at 900 $^{o}$C, DRX occurs at the deformed grain boundaries, and the γ″→δ transformation is accelerated at DRX grain boundary. Consequently, the GB-γ″ nuclei transform into δ phase. Besides, the intragranular γ″ nuclei grow up rapidly, with its morphology changing into disc-shape.

### 3.3 Effects of deformation temperature on precipitation behavior of intragranular γ″-phase

The deformation temperature has great effects on dislocations and diffusion of Nb-atoms within grains. Under the same conditions of strain rate and deformation time, the anomalously coarsening behavior of intragranular γ″-phase in 900-HD specimen can be attributed to the higher deformation temperature than 800-HD specimen. Generally, the slipping and climbing rate of dislocations as well as the diffusion rate of Nb-atoms can be improved by higher deformation temperature. In spite of the weak dynamic recovery effect, the dislocation density within grains of 900-HD is higher than 800-HD specimen. The intragranular higher-density dislocations can lead to the higher nucleation rate and coarsening rate of γ″-phase, as stated above. Hence, it can be concluded that the promoted interaction of dislocations and niobium-diffusion by higher deformation temperature results in the anomalously disc-shaped γ″ precipitates in the grain interior of 900-HD specimen.

### 3.4 XRD results

Fig. 9 demonstrated the diffraction patterns of the two specimens. Obviously, two extra diffraction peaks of δ-phase appear in 900-HD specimen, which are labelled as $(012)_{\delta}$ and $(211)_{\delta}$ respectively [34]. Whereas, only five diffraction peaks of γ-phase are observed in 800-HD specimen. The diffraction patterns are consistent with the above results, which prove that the precipitates at grain boundaries transform from γ″-phase to δ-phase with the deformation temperature increasing from 800 $^{o}$C to 900 $^{o}$C.

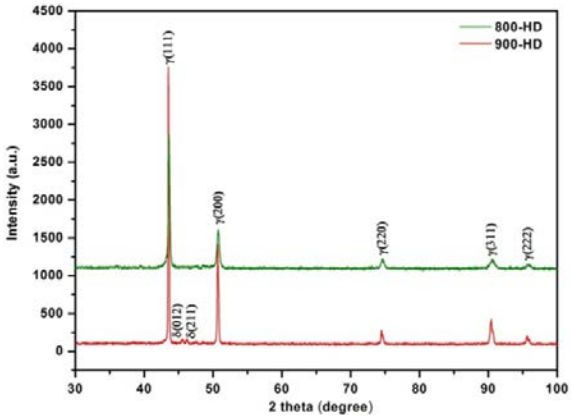


**Fig. 10. Diffraction patterns of two different specimens**

### 3.5 Effects of precipitation behaviors on flow stress

The distinctly varied precipitation behaviors are responsible for the differential flow stress characteristics as demonstrated in Fig. 3. At the initial stage of deformation, dislocations are rapidly generated and accumulated, resulting in the distinct work hardening i.e. the flow stress increases significantly with straining. For 800-HD specimen, the coherence of GB-γ″ phase is gradually reduced during growth, which weakens the grain boundaries. Besides, the nucleation and growth of γ″-phase has consumed lots of dislocations. Consequently, the grain boundary strength is reduced, leading to the decrease of flow stress. When it reaches a dynamic balance between work hardening and γ″-phase coarsening weakness, a peak stress is achieved, and keeps relatively steady in confined range of strain, as indicated in Fig. 3. Afterwards, the flow stress decreases continuously due to the follow-up growth of γ″-phase as well as blocky NbC-carbides precipitating with further straining, resulting in the exceptional flow stress characteristic of 800-HD.

There DRX occurs at the deformation temperature of 900 $^{o}$C, as shown in Fig. 4(b). Hence, the flow stress will be decreased after the peak stress under the effects of DRX coupled with the weak DRV [35]. On the one hand, the volume fraction of DRX is small because of the relatively low recrystallized temperature, which has limited the dynamic softening degree. On the other hand, the δ precipitates will pin the grain boundary and lower its mobility. In addition, the uniformly distributed γ″ precipitates in grain interior can serve as the strengthening phase. Thus, the dynamic softening degree is reduced to a great extent, presenting an unnoticeable dynamic softening feature after peak stress for 900-HD specimen.

## 4. Conclusions

The precipitation behaviors of γ″ and δ phases during hot compressive deformation of the Inconel 718 alloy are investigated under the strain rate of $2.2 \cdot 10^{-4}$ $s^{-1}$ at 800 $^{o}$C and 900 $^{o}$C. Some important conclusions can be summarized as follows:

(1) The true stress-strain curves exhibit two disparately abnormal characteristics. Under the deformation temperature of 800 $^{o}$C which is around the peak temperature of γ″-phase precipitation,

the flow stress decreases apperently after peak stress in the absence of DRX. Whereas, when deformed at 900 °C which is slightly higher than the onset temperature of δ-phase precipitation, the flow stress presents unnoticeable softening after peak stress in spite of a volume fraction of DRX.

(2) The precipitation behaviors are tailored by deformation temperatures. Under the deformation temperature of 800 °C, the microstructure is composed of incoherent needle-shaped γ″ precipitates at grain boundaries and ultrafine spherical γ″ particles within grains. When deformed at 900 °C, it becomes needle-shaped δ precipitates at grain boundaries and intragranular disc-shaped γ″ precipitates.

(3) The distinctly varied precipitation behaviors are responsible for the differential flow stress characteristics. The GB-γ″ phase grows incoherently during deformation at 800°C, resulting in the exceptional decrease of flow stress. At 900 °C, the DRX softening degree is lowered due to the precipitation of GB-δ phase and intragranular coarse γ″ phase.

## Acknowledgments

The authors are grateful to the China National Funds for Distinguished Young Scientists (granted No. 51325401), the National High Technology Research and Development Program of China (Granted No. 2015AA042504), the National Natural Science Foundation of China (Granted No. 51474156) for grant and financial support.

## References

[1] Y. Ning, S. Huang, M.W. Fu, J. Dong. Mater. Charact. 109 (2015) 36-42.
[2] W.C. Liu, F.R. Xiao, M. Yao. Scripta Mater. 37 (1997) 59-64.
[3] H.Y. Zhang, S.H. Zhang, M. Cheng, Z.X. Li. Mater. Charact. 61 (2010) 49-53.
[4] S.A. Nalawade, M. Sundararaman, J.B. Singh, A. Verma, R. Kishore. Mater. Sci. Eng. A 527 (2010) 2906-2909.
[5] K. Wang, M.Q. Li, J. Luo, C. Li. Mater. Sci. Eng. A 528 (2011) 4723-4731.
[6] X.G. Zheng, Y.N. Shi, L.H. Lou. J. Mater. Sci. Technol. 31 (2015) 1151-1157.
[7] Y.C. Lin, D.X. Wen, J. Deng, G. Liu, J. Chen. Mater. Des. 59 (2014) 115–123.
[8] Y. Wang, W.Z. Shao, L. Zhen, B.Y. Zhang. Mater. Sci. Eng. A 528(2011) 3218–3227.
[9] Q.J. Yu, J.H. Liu, W.H. Zhang, L.X. Yu, F. Liu, W.R. Sun, Z.Q. Hu. Rare Met. Mater. Eng. 42 (2013) 1679–1684.
[10] C.G. Yao, B. Wang, D.Q. Yi, B. Wang, X.F. Ding. Mater. Sci. Technol. 30 (2014) 1170–1176.
[11] K. Wu, G.Q. Liu, B.F. Hu, F. Li, Y.W. Zhang, Y. Tao, J.T. Liu, Mater. Des. 32 (2011) 1872–1879.
[12] X.F. Tang, B.Y. Wang, Y.M. Huo, W.Y. Ma, J. Zhou, H.C. Ji, X.B. Fu. Mater. Sci. Eng. A 662 (2016) 54-64.
[13] Y. Wang, L. Zhen, W.Z. Shao, L. Yang, X.M. Zhang. J. Alloy Compd. 474(2009) 341-346.
[14] H. Yuan, W.C. Liu. Mater. Sci. Eng. A 408(2005) 281-289.

[15] Y.Q. Ning, Z.K. Yao, Y.Y. Lei, H.Z. Guo, M.W. Fu. Mater. Charact. 62 (2011) 887–893.
[16] D.X. Wen, Y.C. Lin, H.B. Li, X.M. Chen, J. Deng, L.T. Li, Mater. Sci. Eng. A 591(2014) 183–192.
[17] T. Liu, J.S. Dong, L. Wang, Z.J. Li, X.T. Zhou, L.H. Lou, J. Zhang. J. Mater. Sci. Technol. 31 (2015) 269-279.
[18] Y.C. Lin, X.M. Chen. Mater. Des. 32(2011) 1733-1759.
[19] N. Nayan, N.P. Gurao, S.V.S.N. Murty, A.K. Jha, B. Pant, K.M. George. Mater. Charact. 110 (2015) 236-241.
[20] X.M. Chen, Y.C. Lin, D.X Wen, J.L. Zhang, M. He. Mater. Des. 57 (2014) 568-577.
[21]A.Niang, B.Viguier, J. Lacaze. Mater. Charact. 61 (2010) 525-534.
[22] Y.P. Mei, Y.C. Liu, C.X. Liu, C. Li, L.M. Yu, Q.Y. Guo, H.J. Li. J. Alloy Compd. 649(2015) 949-960.
[23]X.M. Chen, Y.C. Lin, M.S. Chen, H.B. Li, D.X. Wen, J.L. Zhang, M. He. Mater. Des. 77(2015) 41-49
[24]M. Fisk, J. Andersson, R.D. Rietz, S. Haas, S. Hall. Mater. Sci. Eng. A 612 (2014) 202-207
[25] I.M. Lifshitz, V.V. Slyozov, J. Phys. Chem. Solids. 19 (1961) 35.
[26] S. Tang, L.K. Ning, T.Z. Xin, Z. Zheng. J. Mater. Sci. Technol. 32 (2016) 172-176.
[27] T. Grosdidier, A. Hazotte, A. Simon. Mater. Sci. Eng. A 256 (1998) 183–196.
[28] C.S. Wang, Y.A. Guo, J.T. Guo, L.Z. Zhou. Mater. Sci. Eng. A 670 (2016) 178–187.
[29]A. Devaus, L. Naze´, R. Molins, A. Pineau, A. Organista, J.Y. Gue´dou, J.F. Uginet, P. He´ritier. Mater. Sci. Eng. A 486 (2008) 117–122.
[30] C. Slama, C. Servant, G. Cizeron. J. Mater. Res. 12 (1997) 2298.
[31] D.X. Wen, Y.C. Lin, J. Chen, X.M. Chen, J.L. Zhang, Y.J. Liang, L.T. Li. J. Alloy Compd. 618(2015) 372–379.
[32] A. Thomas, M.E. Wahabi, J.M. Cabrera, J.M. Prado. J. Mater. Process. Tech. 177 (2006) 469-472.
[33] X.D. Lu, J.H. Du, Q. Deng. Mater. Sci. Eng. A 559 (2013) 623–628.
[34] W.C. Liu, F.R. Xiao, M. Yao. J. Mater. Sci. Lett. 16(1997) 769-771.
[35] H. Riedel, J. Svoboda. Mater. Sci. Eng. A 665 (2016) 175–183.